



Superior UVC light-mediated catalytic activity of a novel NiFe₂O₄@TiO₂ magnetic nanocomposite synthesized with green route using *Pulicaria Gnaphalodes* plant extract for enhanced photocatalytic degradation of an antibiotic in water solution

Elham Derakhshani¹ · Ali Naghizadeh¹ · Sobhan Mortazavi-Derazkola¹

Received: 22 August 2023 / Accepted: 1 December 2023 / Published online: 9 January 2024
© The Author(s) 2024

Abstract

In this study, the NiFe₂O₄@TiO₂ magnetic nanocomposite was synthesized by the green synthesis method, which is an efficient and economical method. *Pulicaria Gnaphalodes* plant extract was used for nanocomposite synthesis because this method is suitable for the biosynthesis of nanocomposites on a large scale, and the nanocomposite produced by plants is more stable. The efficiency of the synthesized nanocomposite was investigated for the photocatalytic degradation of Penicillin G (PNG) under UVC light irradiation in aqueous solutions. The structural characteristics of this nanocomposite were determined by field emission scanning electron microscopy, transmission electron microscopy, X-ray diffraction, Fourier transform infrared spectroscopy, vibrating sample magnetometer, and dynamic light scattering. The effect of different parameters including pH, nanocomposite dose, penicillin G concentration and time were studied to reach optimum conditions. About 71% of PNG in optimal conditions (pH=9, nanocomposite dose=0.6 g/L, and penicillin G concentration=10 mg/L) was decomposed. Generally, the NiFe₂O₄@TiO₂ nanocomposite can be used as an efficient catalyst for the degradation of PNG in aqueous solutions.

Keywords NiFe₂O₄ · TiO₂ · Green synthesis · Photocatalytic · Penicillin G

Introduction

In recent decades, pharmaceutical compounds, especially antibiotics, have been considered as one of the most important aqueous solution pollutants. Because antibiotics are widely used to treat human and animal infectious diseases and have high stability in the environment, high residual toxicity, high solubility in water and are non-biodegradable (Wang and Zhuan 2020; Kamranifar et al. 2019b; Ouaisa et al. 2014). Medicinal compounds enter water resources through various sources such as wastewater from hospitals and homes, pharmaceutical factories, and animal husbandry units (Elmolla and Chaudhuri 2010). Antibiotics are compounds obtained from microorganisms and have bactericidal

or bacteriostatic properties. These compounds affect bacteria, especially pathogens, and only a small percentage of them change in the body, and the rest are excreted unchanged from the human body. Antibiotics with low concentrations cause antibiotic resistance in pathogenic bacteria which is why they are so important (Qin et al. 2021; Ahmed et al. 2015). One of the important classifications of antibiotics is based on the presence of beta-lactam rings in their structure. Beta-lactam antibiotics are a broad group of antibiotics that have a beta-lactam ring in their molecular structure. Antibiotics of this group include penicillins, cephalosporins, monobactams and carbapenems (Lima et al. 2020; Kamranifar et al. 2019b). One of the most important groups of beta-lactam antibiotics is penicillins, which are used against sensitive organisms, especially gram-positive bacteria, and often affect the cell wall of bacteria (Salehnia et al. 2020). The results of previous research show that antibiotics are not completely removed in sewage treatment plants and enter the water environment; also, the presence of these compounds in the sludge of sewage treatment plants has been

✉ Ali Naghizadeh
al.naghizadeh@yahoo.com

¹ Medical Toxicology and Drug abuse Research Center (MTDRC), Birjand University of Medical Sciences (BUMS), Birjand, Iran

proven. Because antibiotics damage the microbes active in the purification and cause the lack of proper purification, it is very important to remove them from the wastewater before it is discharged into the biological purification process and receiving water (Aksu and Dede 2005; Gulkowska et al. 2008; Seifrtová et al. 2009). Various methods such as membrane separation (Sui et al. 2010), advanced oxidation processes (Anirudhan et al. 2021; Naghizadeh et al. 2017), ozonation (Sun et al. 2012), surface adsorption (Kamranifar et al. 2019a), biodegradation (Wang and Zhuan 2020), electrocoagulation (Arsand et al. 2013), and photolysis (Wammer et al. 2013) have been used to remove drugs and antibiotics from aqueous solutions. In recent years, the use of advanced oxidation processes (AOPs) has been recognized as a useful method for purifying aqueous solutions. The mechanism of advanced oxidation processes (AOPs) is based on the production of highly reactive species, such as hydroxyl radicals ($\cdot\text{OH}$). In this process, by using various methods such as ozone, ultraviolet rays, and H_2O_2 , a combination of them tries to produce free radicals and use them to remove all kinds of pollutants in aqueous solutions. Hydroxyl free radicals are highly reactive due to having free electrons (Derakhshani et al. 2023b; Basha et al. 2011; Singh et al. 2023; Naghizadeh et al. 2015). One of the advanced oxidation processes is the photocatalytic process, which is widely used in the purification of aqueous solutions due to its high degradation potential, relatively short reaction time, and mild reaction conditions (Darvishi Cheshmeh Soltani et al. 2015). Semiconductor ferrites (MFe_2O_4) are widely used for environmental applications due to their unique physical and chemical properties and specific magnetic bonds at the nanometer scale. These semiconductor materials must have special properties to be used as photocatalysts in studies, including high optical activity, chemical stability, unique electronic properties, low-cost, and high oxidizing properties (Derakhshani et al. 2023a; Sanadi et al. 2021). Among semiconductor ferrites, nickel ferrite nanocomposite (NiFe_2O_4) is used in various fields, especially as photocatalysts, due to its chemical stability, electrocatalytic behavior, and unique magnetic structure (Makofane et al. 2022; Sivakumar et al. 2013). Modifying the surface of nickel ferrite nanocomposite (NiFe_2O_4) by various compounds such as TiO_2 improves their performance in removing pollutants from aqueous solutions (Poursaberi et al. 2012). TiO_2 is a primary semiconductor and can be considered one of the best photocatalyst materials, because it is a non-toxic material and has high oxidation power and chemical stability (Karmakar et al. 2018). So far, various methods have been used for the synthesis of nickel ferrite nanoparticles, the common types of which include: the co-precipitation method (Sivakumar et al. 2011), hydrothermal technique (Li et al. 2010), sol-gel method (Malik et al. 2010), microwave plasma (Bousquet-Berthelin et al. 2008), electrochemical

synthesis (Zhao et al. 2007), solvothermal method (Yan et al. 2010), and micro-emulsion process (Hirai et al. 1999). Some of the above methods cause problems such as increasing impurity and toxicity of nanoparticles, creating dangerous side products, and environmental pollution, and also leading to the production of nanoparticles with non-uniform size (Hussain et al. 2016; Saif et al. 2016). Therefore, researchers have made many efforts to synthesize nanoparticles through an environmentally friendly process using enzymes, microscopic organisms, and plant extracts, which is called green synthesis. This method of synthesis of nanoparticles has advantages over other methods, which include producing more stable materials, not using toxic and dangerous chemicals, being cost-effective, and being environmentally friendly (Kulkarni et al. 2020). Green synthesis of nanoparticles is the most effective way of minimizing the use of toxic chemicals and the formation of their toxic by-products. Green nanoparticles have a maximum level of antimicrobial effects with minimal toxicity.

In this study, $\text{NiFe}_2\text{O}_4@\text{TiO}_2$ magnetic nanocomposite was produced by green synthesis using *Pulicaria Gnaphalodes* plant extract and used to remove PNG from aqueous solutions, and the effect of parameters such as pH, nanocomposite dose, PNG concentration, and contact time were investigated. The reason why this plant was used for green synthesis is its distribution and abundance around South Khorasan province in Iran (where this research was conducted). According to the unique characteristics of this plant and according to the previous studies of the researchers of this article, it was used as a suitable candidate for the reducing and capping agent in the synthesis process of NiFe_2O_4 nanoparticles.

Materials and methods

Materials

PNG powder was purchased from Sigma-Aldrich, and a stock solution with a concentration of 500 mg/L was prepared using double distilled water. Other chemicals used in this study include Iron Nitrate Hexahydrate ($\text{Fe}(\text{NO}_3)_3 \cdot 9\text{H}_2\text{O}$), Nickel Chloride salt ($\text{NiCl}_2 \cdot 6\text{H}_2\text{O}$), SDS surfactant, Tetra-n-Butyl Titanate solution ($(\text{CH}_3\text{CH}_2\text{CH}_2\text{CH}_2\text{O})_4\text{Ti}$), Sodium Hydroxide (NaOH), Hydrochloric acid (HCl), methanol, and ethanol from Merck (Germany) was purchased. A UV-C lamp (Philips, Poland) with a power consumption of 9 watts, a production wavelength of 253.7 nm, a radiation intensity of 282–294 W/m^2 and a length of 22 cm and diameter of 2 cm was used and installed in the center of the reactor.

Preparation of methanolic plant extract

To synthesize $\text{NiFe}_2\text{O}_4@ \text{TiO}_2$, the *Pulicaria Gnaphalodes* plant was collected from around Birjand city (the capital of the South Khorasan province of Iran) and transported to the laboratory. After washing three times with distilled water, this plant was placed at room temperature to dry. To prepare the extract, some of the dried powder of the plant was contacted with a methanol solution and then the solution was passed through Whatman No. 42 paper. A rotary vacuum evaporator (Hei zbad WB eoc, Germany) was used to concentrate methanol and separate the extract.

Biosynthesis of $\text{NiFe}_2\text{O}_4@ \text{TiO}_2$ nanocomposite

First, 5 g of Iron Nitrate Hexahydrate ($\text{Fe}(\text{NO}_3)_3 \cdot 9\text{H}_2\text{O}$) was added to 70 mL of deionized water and dissolved in water under nitrogen gas conditions for 1 h. In another container, SDS surfactant (1:1 molar ratio to iron salt) was dissolved in 30 mL of distilled water and added to the iron salt as a covering agent. The reaction was continued for 30 min under vigorous stirring at room temperature. Then, 1.47 g of Nickel Chloride salt ($\text{NiCl}_2 \cdot 6\text{H}_2\text{O}$) was added to the reaction solution, and 2 M Sodium Hydroxide was added to increase the pH of the reaction to 12. After 2 h, the sediments obtained were washed and dried after centrifugation at room temperature for 24 h. NiFe_2O_4 nanocomposite was obtained by calcining the deposits at 600°C for 3 h.

The synthesis of $\text{NiFe}_2\text{O}_4@ \text{TiO}_2$ nanocomposite was carried out by sonication of 0.2 g of NiFe_2O_4 nanocomposite in 25 mL of deionized water and ethanol solutions. Then, 1

mL of Tetra-N-Butyl Titanate solution was added drop by drop to the reaction solution under magnetic stirring conditions. After 30 min, the pH of the reaction reached 2 with the addition of 2 M NaOH. The reaction continued at room temperature for 3 h. Finally, the sediments obtained were washed with distilled water and ethanol. The deposits were dried in an oven for 24 h. The final product was obtained by calcining the sediments obtained at 600°C for 3 h. Schematics of methanolic extraction of *Pulicaria Gnaphalodes* plant as well as the green synthesis of $\text{NiFe}_2\text{O}_4@ \text{TiO}_2$ are shown in Figs. 1 and 2, respectively.

Measurements of pHzpc for $\text{NiFe}_2\text{O}_4@ \text{TiO}_2$

To determine the point of zero charge (pH_{zpc}) of $\text{NiFe}_2\text{O}_4@ \text{TiO}_2$ magnetic nanocomposite, 11 Erlenmeyer flasks with 50 mL of distilled water were used. Then, the initial pH of the containers was adjusted between 2 and 12 using 1 M NaOH and HCl solutions. Afterward, 0.25 g of the synthesized nanocomposite was added to Erlenmeyer flasks and placed on a shaker for 24 h. The pH of the containers was measured again and a graph of initial pH was plotted against final pH. Finally, the intersection point of two pH_{zpc} curves was introduced.

Photocatalytic experiments

PNG photocatalytic reaction experiments were performed using $\text{NiFe}_2\text{O}_4@ \text{TiO}_2$ magnetic nanocomposites in a photochemical reactor with an internal chamber of 100 mL. PNG powder was used to prepare a stock solution with a

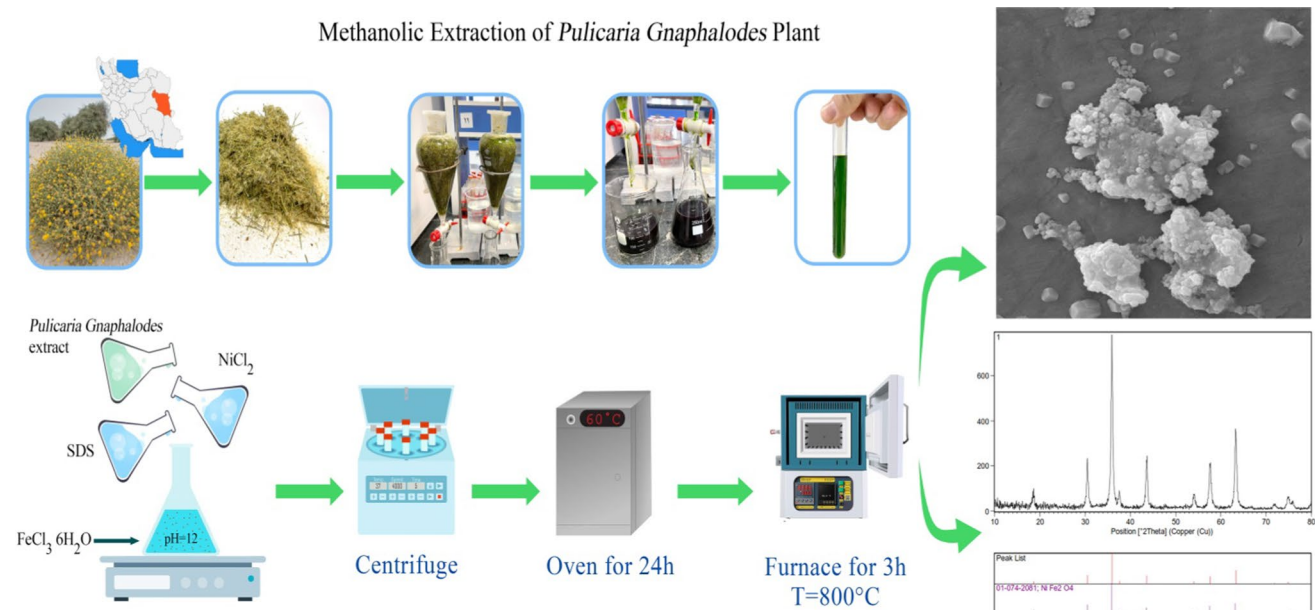


Fig. 1 Methanolic Extraction of *Pulicaria Gnaphalodes* plant and NiFe_2O_4 synthesis

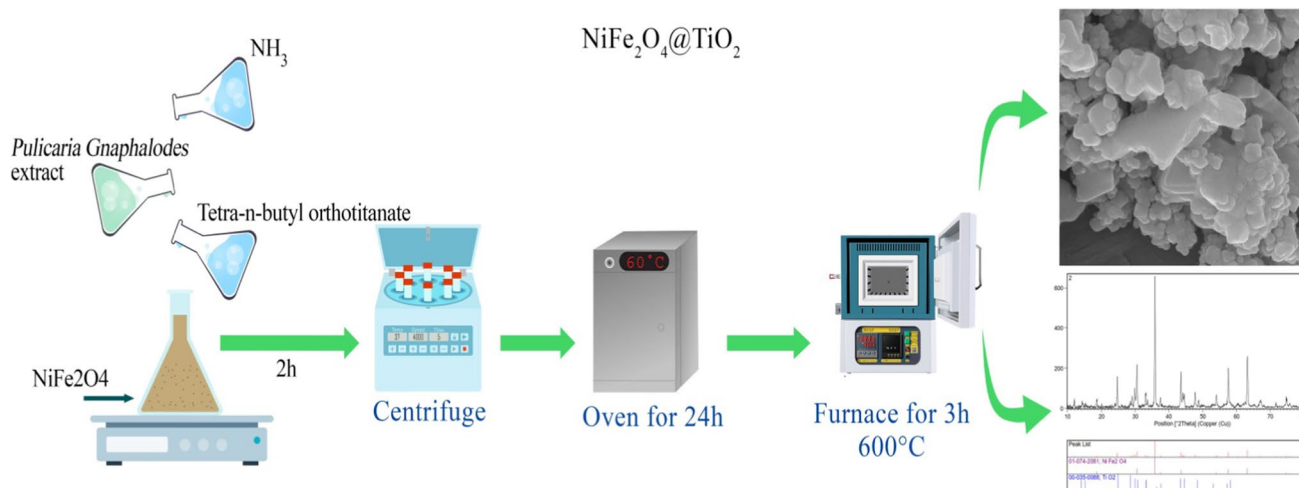


Fig. 2 Green synthesis of $\text{NiFe}_2\text{O}_4@\text{TiO}_2$ with *Pulicaria Gnaphalodes* plant methanolic extract

concentration of 500 mg/L, and other initial concentrations of the solution were made by diluting the stock solution. To avoid the influence of other lights, all PNG solutions were kept in dark conditions. In addition, the body of the photoreactor was made from stainless steel. PNG removal efficiency in the photocatalytic process using $\text{NiFe}_2\text{O}_4@\text{TiO}_2$ nanocomposite in different pH ranges (3, 5, 7, 9, 11), PNG concentrations (10, 20, 30, 50, 70 mg/L), nanocomposite doses (0.1, 0.2, 0.4, 0.6, 0.8, and 1.25 g/L), and contact times (10, 20, 40, 60, 100, and 120 min) were investigated at temperature of 25 °C. The flasks were kept in dark conditions for about 30 min with no UV-C radiation before starting the photocatalytic process. At different time intervals of irradiation, 5 mL of reacted PNG solution was taken and centrifuged at a speed of 6000 rpm for 8 min to completely separate the nanocatalyst particles from the solution. The initial and residual concentrations of PNG in the tested samples were measured using a UV spectrophotometer (T80, UV/Visible, England) at a spectral peak of 254 nm. PNG removal efficiency (%R) was determined using the following equation:

$$R = \frac{C_0 - C_t}{C_0} \times 100$$

where C_0 is the initial concentration of PNG (mg/L) before the photocatalytic process, and C_t is the residual concentration of PNG after the process.

Results and discussion

Characteristics of the $\text{NiFe}_2\text{O}_4@\text{TiO}_2$ magnetic nanocomposite

FTIR analysis

FTIR analysis revealed the presence of distinct chemical bonds within the nanocomposite. Specifically, it confirmed the presence of titanium–oxygen bonds, carbon–carbon bonds, and Mn–O bonds. This provides evidence of the composition and chemical integrity of the nanocomposite. Figure 3 illustrates the FTIR spectra of $\text{NiFe}_2\text{O}_4@\text{TiO}_2$. The absorption band at about 3420 cm^{-1} is related to the stretching mode of the hydroxyl groups (OH) on the surface of the $\text{NiFe}_2\text{O}_4@\text{TiO}_2$. A band observed at 563 cm^{-1} is assigned to the stretching vibrations of Ti–O in anatase TiO_2 (Li et al. 2015). According to the synthesis results, $\text{NiFe}_2\text{O}_4@\text{TiO}_2$ nanocomposites have been successfully synthesized.

XRD analysis

The structural and crystalline properties of the products were examined using X-ray diffraction (XRD) analysis. Figure 4 displays the XRD patterns specifically for the

Fig. 3 FTIR spectrum of $\text{NiFe}_2\text{O}_4@/\text{TiO}_2$

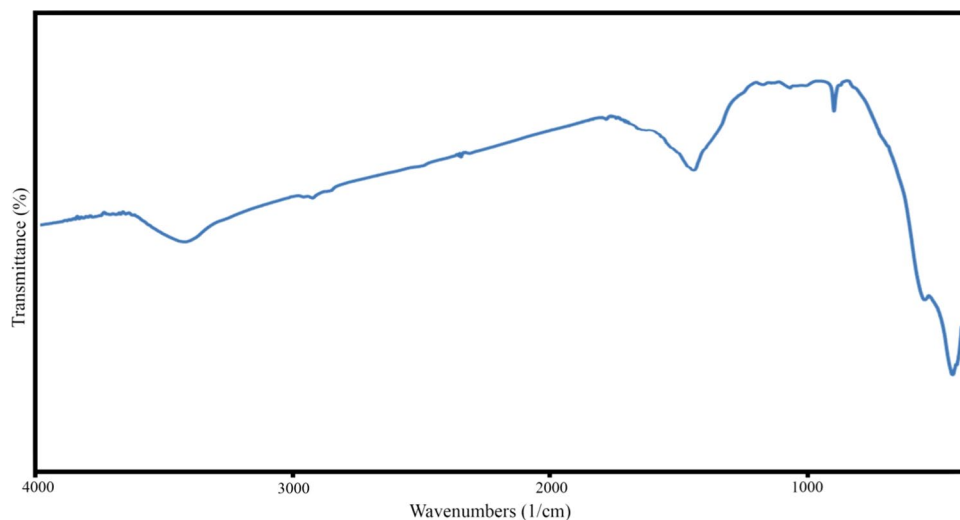
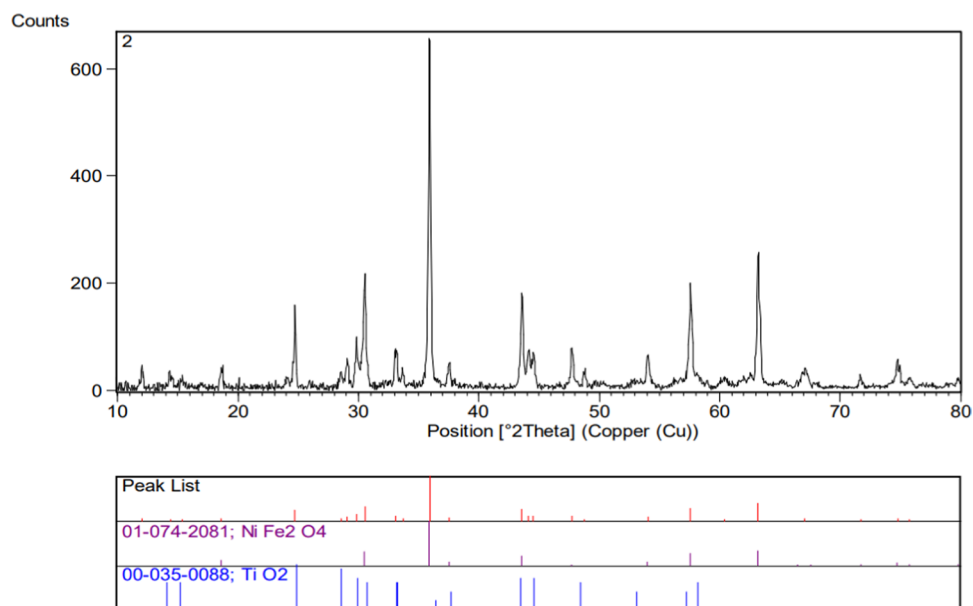


Fig. 4 XRD pattern of $\text{NiFe}_2\text{O}_4@/\text{TiO}_2$



$\text{NiFe}_2\text{O}_4@/\text{TiO}_2$ nanoparticles. XRD analysis successfully characterized the crystal structure of the $\text{NiFe}_2\text{O}_4@/\text{TiO}_2$ magnetic nanocomposite. The diffraction patterns obtained confirmed the crystalline nature of the material and allowed for the determination of crystal lattice parameters, crystal size, and the identification of phases present. The patterns shown in Fig. 4 can be easily identified as anatase titania based on the presence of peaks at 2θ values of 25.4, 38.1, and 48.2° [JCPDS card no 00-035-0088], which correspond to the (101), (004), and (200) crystallographic planes, respectively. These findings indicate that the $\text{NiFe}_2\text{O}_4@/\text{TiO}_2$ nanoparticles consist of a layer of TiO_2 covering the NiFe_2O_4 nanoparticles, as there were no distinct peaks solely attributed to NiFe_2O_4 present. Our findings align with the research conducted by Kim and colleagues (Kim et al. 2014).

FESEM and EDS mapping analysis

The composites that were prepared underwent analysis of their surface characteristics and structure using a scanning electron microscope (SEM). SEM images, presented in Fig. 5, depict the modified NiFe_2O_4 nanoparticles with TiO_2 , accompanied by elemental mapping conducted through magnetic particles. Figure 6 displays the SEM-EDS spectrum of the $\text{NiFe}_2\text{O}_4@/\text{TiO}_2$ composite, providing further analysis. The EDS spectrum and elemental mapping confirm the successful coating of the NiFe_2O_4 particles with TiO_2 , demonstrating the presence and even distribution of Ni, Ti, Fe, and O. energy dispersive spectroscopy (EDS). Figure 5 reveals the rough surface texture of the NiFe_2O_4 spheres, indicating the existence of a TiO_2 layer on their surfaces. Upon closer examination, the images also illustrate the spherical shape

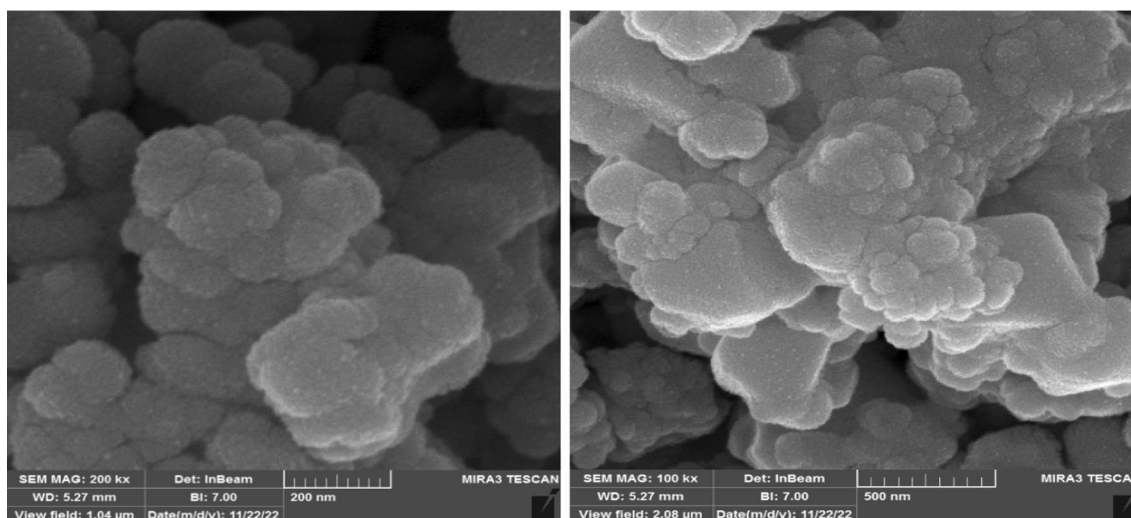
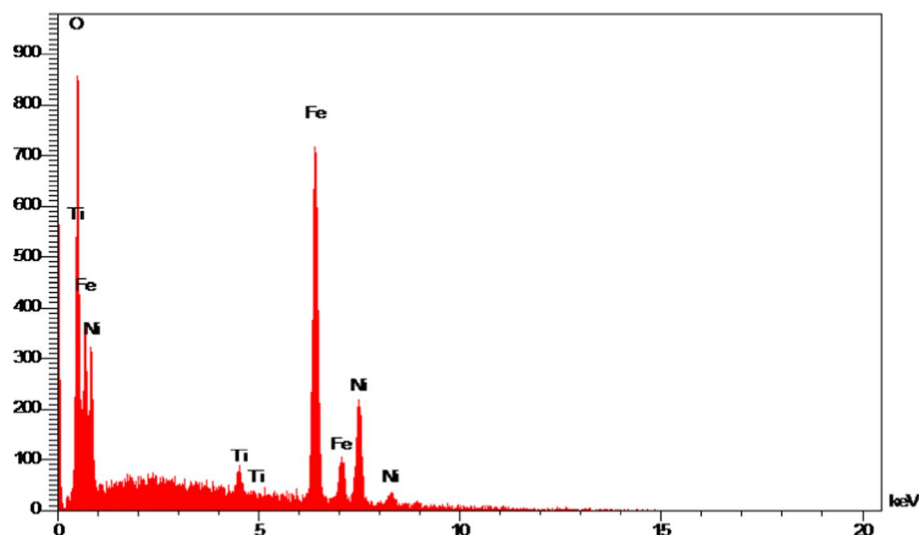


Fig. 5 FESEM Spectra of NiFe₂O₄@TiO₂ nanocomposite

Fig. 6 EDS curve of NiFe₂O₄@TiO₂ nanocomposite



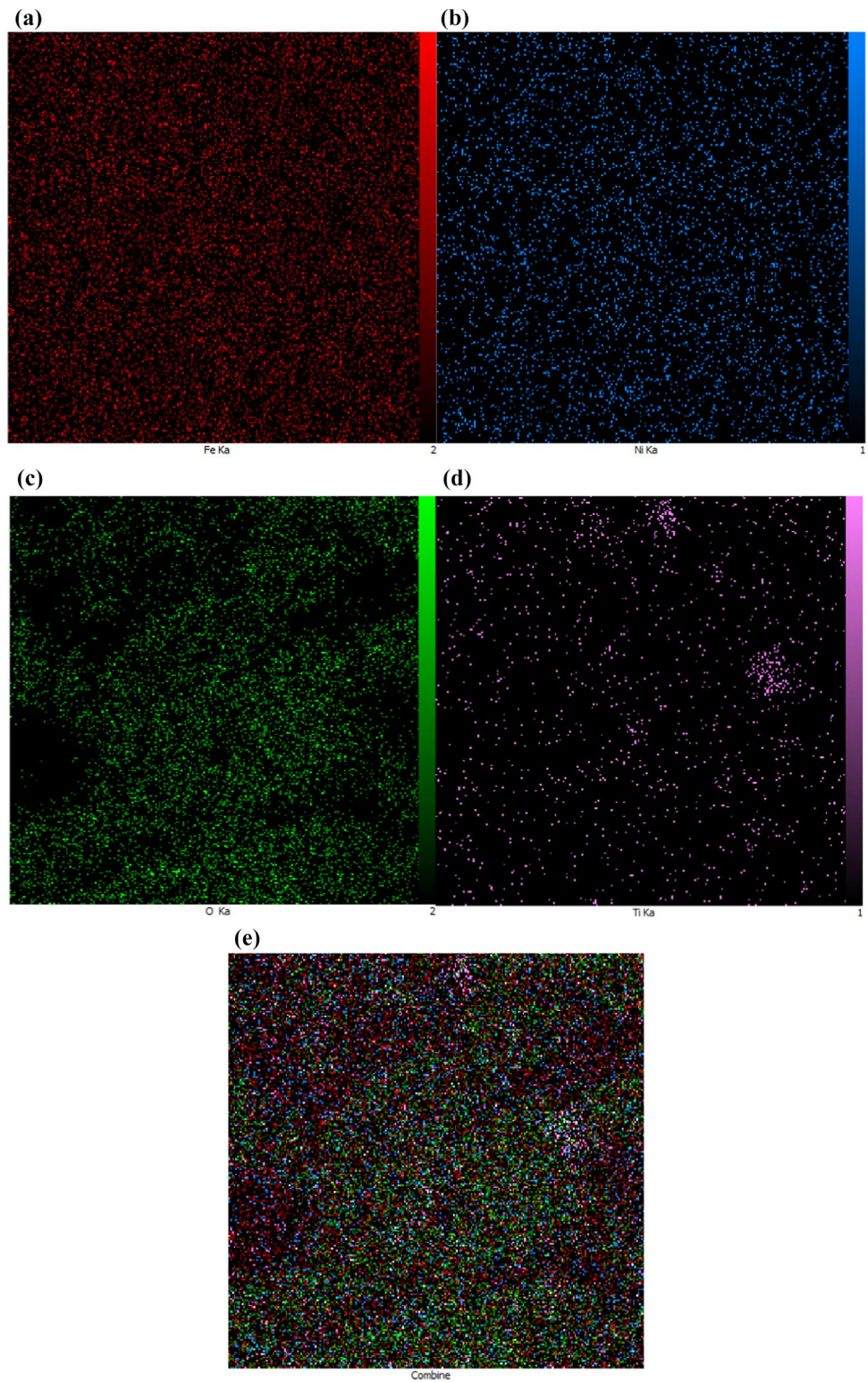
of the particles. Furthermore, there is variation in particle sizes, with some larger particles likely formed due to the aggregation of smaller ones. EDS mapping analysis visualizes the distribution of the constituent elements in the nanocomposite by two dimensionally displaying the characteristic X-ray intensities or the concentrations of the elements (Esmati et al. 2021). Based on the results of this analysis (Fig. 6), nickel, iron, titanium, and oxygen elements were uniformly distributed. Mapping spectra of NiFe₂O₄@TiO₂ nanocomposite including each constituent element alone and combined are shown in Fig. 7.

VSM analysis

One of the most important properties of nanocomposites is their magnetic property, which is studied using VSM

analysis. This analysis is done by a vibrating sample magnetometer. Several parameters including the material's residual loop, can be obtained through the interpretation of VSM analysis results. The VSM analysis demonstrated the magnetic properties of the NiFe₂O₄@TiO₂ nanocomposite. It indicated the presence of a suitable magnetic structure, offering insights into the material's potential applications in magnetic devices or separations. In summary, the amalgamation of these characterization techniques allowed us to comprehensively assess the structural attributes of the NiFe₂O₄@TiO₂ nanocomposite. Figure 8 shows the hysteresis ring of magnetic nanocomposite NiFe₂O₄ and NiFe₂O₄@TiO₂ obtained at room temperature. Based on these two curves, the saturation magnetization (M_s) value for NiFe₂O₄ and NiFe₂O₄@TiO₂ is 25.6 emu/g and 23 emu/g, respectively, and by comparing them, we conclude

Fig. 7 Mapping spectra of NiFe₂O₄@TiO₂ nanocomposite
a Fe Ka, **b** Ni Ka, **c** O Ka, **d** Ti Ka
e combine



that the magnetic property of NiFe₂O₄ decreases with its surface modification. Based on these magnetic properties of the nanoparticles, this compound shows promise as a suitable option for use as a recyclable catalyst.

DLS analysis

Zeta potential distribution and dynamic light scattering (DLS) analyses were performed to investigate the

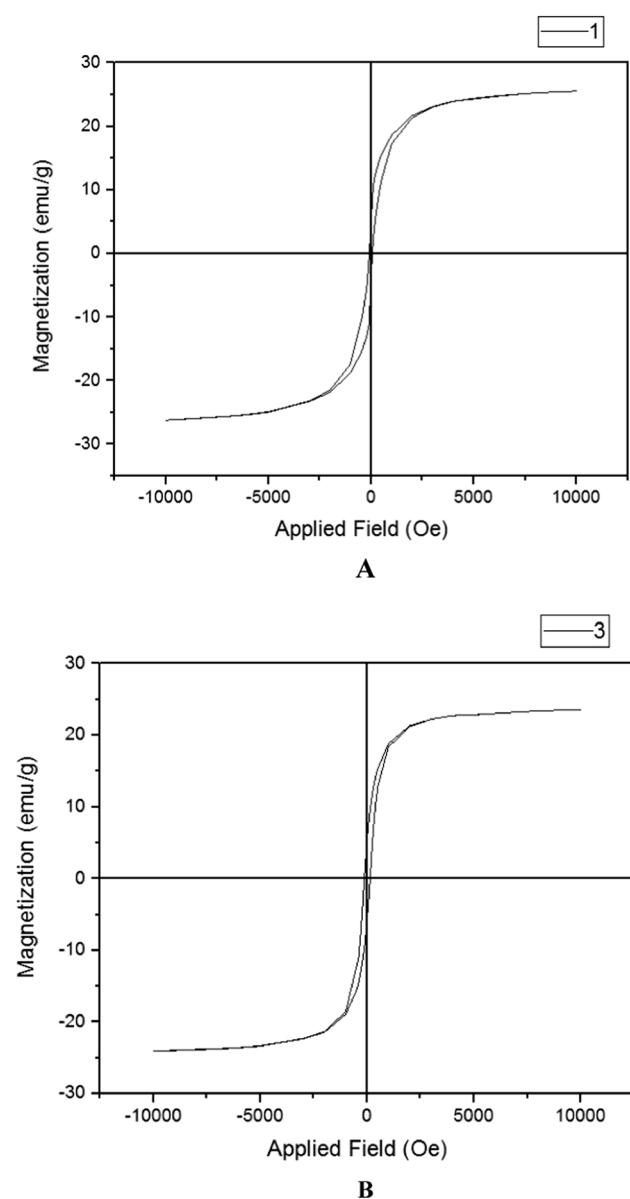


Fig. 8 VSM analysis of **A** NiFe₂O₄ **B** NiFe₂O₄@TiO₂ nanocomposite

stabilization and size distribution of biosynthesized NiFe₂O₄@TiO₂ nanocomposites (Fig. 9). The DLS analysis exhibited the hydrodynamic size of NiFe₂O₄@TiO₂ nanocomposites as 80–110 nm (Fig. 7). The colloidal solution of NiFe₂O₄@TiO₂ nanocomposites had a high negative zeta potential of about -5.4 mV, which indicates that the biosynthesized NiFe₂O₄@TiO₂ nanocomposites were highly stable.

TEM analysis

TEM imaging unveiled the morphological characteristics of the nanocomposite. It exhibited a spherical structure, thus establishing the nano-sized nature of the particles. This detailed information about particle size and shape is

critical in understanding the nanocomposite's properties. TEM image of NiFe₂O₄@TiO₂ magnetic nanocomposite is shown in Fig. 10. According to this image the size of the synthesized nanocomposite is lower than 100 nm. The TEM analysis or transmission electron microscope is one of the most important analysis methods for studying materials, especially nanostructured materials, due to its extremely high ability to image particles at magnifications of nearly one million times. Using TEM analysis, it is possible to study the microstructure of materials, observe nanoparticles and examine their internal structure. This microscope is the most powerful tool for imaging materials and along with SEM and AFM analysis methods, a complete study of nanostructured materials can be done.

Measurements of point of zero charge (pH_{zpc})

pH_{zpc} is generally described as the pH at which the total net charge of the nanocomposite surface is zero and neutral. Figure 11 shows that the pH_{zpc} of NiFe₂O₄@TiO₂ magnetic nanocomposite is about 6.7. The nanocomposite surface has a positive charge at pH < pH_{zpc} and a negative charge at pH > pH_{zpc}.

Effect of pH

Figure 12 shows the effect of pH 3, 5, 7, 9, and 11 on the photocatalytic degradation of PNG by NiFe₂O₄@TiO₂ magnetic nanocomposite. PNG solution with a concentration of 20 mg/L was prepared for this experiment and after pH adjustment, 0.6 g/L of catalyst was added to it and the tests were performed. The maximum amount of photocatalytic degradation of PNG occurred at pH = 11. Considering that the percentage of removal is close at pH 9 and 11, and considering that operationally, a lot of alkali is used to bring the pH from 9 to 11, we chose pH 9. Therefore pH = 9 was selected as the optimal pH.

As the pH increases from 3 to 11, the degradation rate of PNG decreases. Solution pH is one of the factors affecting the efficiency of advanced oxidation processes, especially photocatalytic degradation, which affects the surface charge of photocatalysts, the solubility of antibiotics, and the mechanism of hydroxyl radical production (Dehghani et al. 2014). PNG has the highest decomposition rate in an alkaline medium. In the alkaline environment, there are more hydroxide ions (OH⁻) on the surface of nanoparticles, which are easily oxidized and form hydroxyl radicals (OH) with a very high oxidation potential. On the other hand, in alkaline environments, the hydrolysis of antibiotics takes place due to the instability of the β-lactam ring. Therefore, nanoparticles can react more effectively with PNG molecules and cause their destruction (Elmolla and Chaudhuri 2010; Pandey et al. 2023).

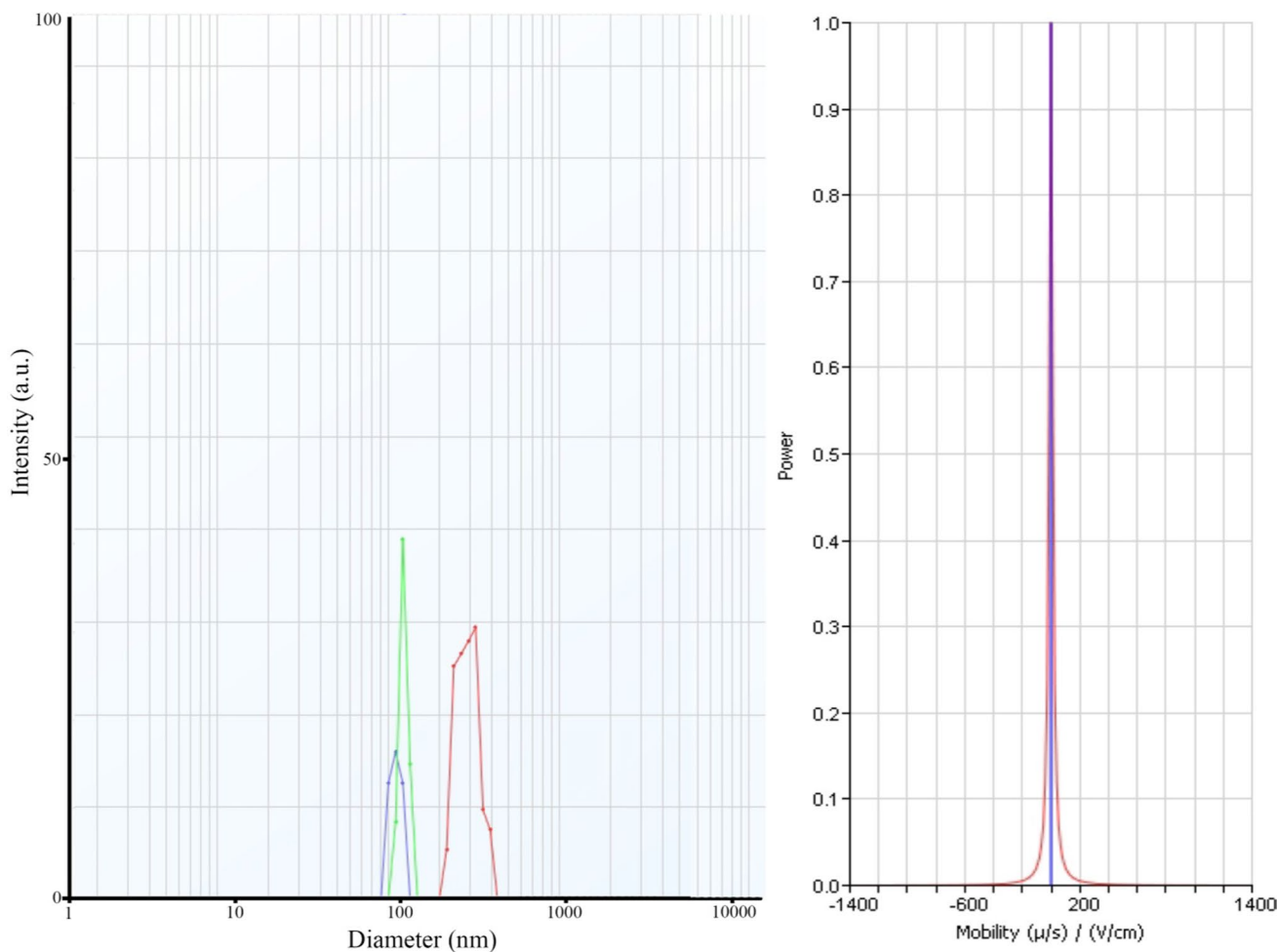


Fig. 9 DLS graph of $\text{NiFe}_2\text{O}_4@\text{TiO}_2$ nanocomposite

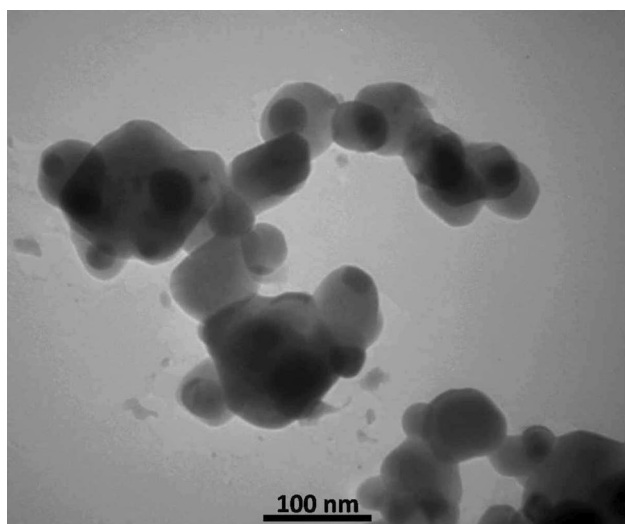


Fig. 10 TEM image of $\text{NiFe}_2\text{O}_4@\text{TiO}_2$ nanocomposite

Effect of nanocatalyst dosage

The effect of $\text{NiFe}_2\text{O}_4@\text{TiO}_2$ nanocatalyst dosage on PNG decomposition was investigated in the range of 0.8–1.25 g/L at pH=9 and a concentration of 20 mg/L of PNG and a temperature of 25 °C (Fig. 13). Experiments performed with different dosages of $\text{NiFe}_2\text{O}_4@\text{TiO}_2$ magnetic nanocomposite showed that the photocatalytic degradation of PNG increases with increasing the catalyst dosage up to 0.6 g/L and then decreases. The highest degradation of PNG was observed in the nanocomposite dose of 0.6 g/L with a degradation percentage of 65.50%.

By increasing the dose of photocatalyst, the number of active sites on the surface of the catalyst increases, which leads to the production of more hydroxyl radicals, and as a result, the photocatalytic degradation efficiency of PNG increases. But further increase in the dose of photocatalyst leads to the accumulation of $\text{NiFe}_2\text{O}_4@\text{TiO}_2$ and increasing the turbidity of the solution. The created turbidity reduces the penetration of UV light into the solution and

Fig. 11 pH_{zpc} of magnetic $NiFe_2O_4@TiO_2$ nanocomposite

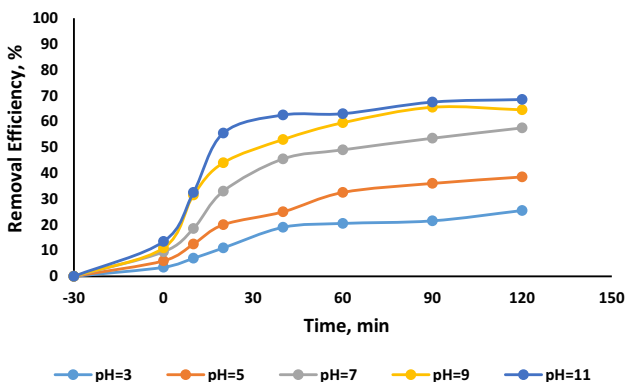
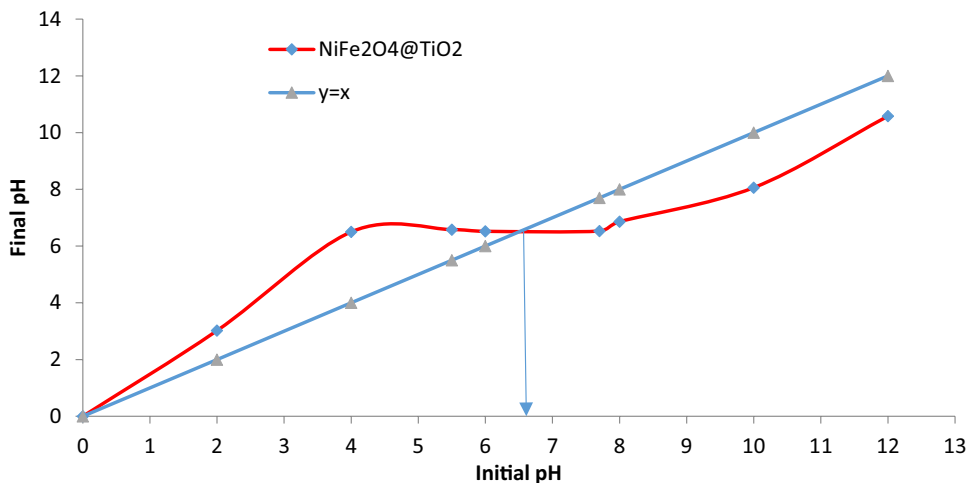


Fig. 12 Effect of solution pH on photocatalytic efficiency of PNG by $NiFe_2O_4@TiO_2$ ($C_0=20$ mg/L, Nano catalyst dosage=0.6 g/L, $T=25$ °C)

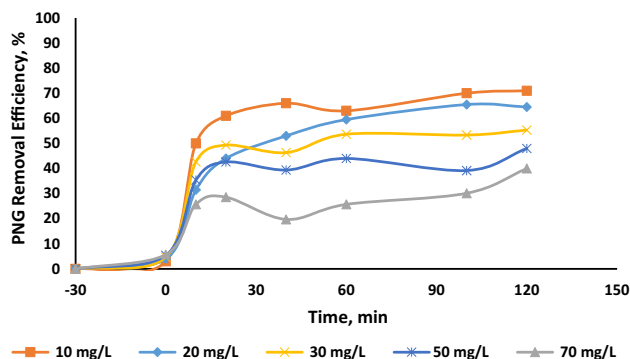


Fig. 14 Effect of initial PNG concentration and contact time on photocatalytic efficiency of PNG by $NiFe_2O_4@TiO_2$ (Nano catalyst dosage=0.6 g/L, $pH=9$, $T=25$ °C)

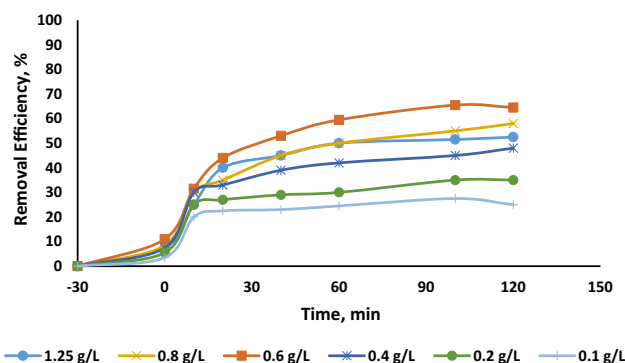


Fig. 13 Effect of nanocatalyst dosage on photocatalytic efficiency of PNG by $NiFe_2O_4@TiO_2$ ($C_0=20$ mg/L, $pH=9$, $T=25$ °C)

light scattering, thus reducing the degradation rate of PNG (Geng et al. 2019). In a study, Wang et al. used zinc titanate nanoparticles for the photocatalytic degradation of humic acid in water, they concluded that the light scattering action

is intensified by the overly suspended catalyst in the aqueous solution, which leads to a decrease in the photocatalytic activity (Wang et al. 2012; Alam et al. 2017).

Effect of initial PNG concentration and contact time

Figure 14 shows the effect of the initial concentration of PNG and the contact time. To investigate the effect of the initial concentration of PNG on its photocatalytic degradation using $NiFe_2O_4@TiO_2$ nanocomposites, the concentration of PNG in the range of 10 to 70 mg/L in different contact times was investigated. As shown in Fig. 14, increasing the concentration of PNG decreases the degradation efficiency.

A higher concentration of PNG acts as a barrier against the transmission of ultraviolet light to reach the catalyst surface and, as a result, reduces the activation of the catalyst and insufficient oxidation of PNG. On the other hand, the number of hydroxyl radicals produced for higher PNG concentrations is not enough, because the number of these radicals is constant, but the pollutant concentration increases.

Therefore, increasing the concentration of PNG leads to an inhibitory effect on its destruction (Moradi et al. 2018) (Alam et al. 2018).

The reaction time is one of the important and influential parameters in the process of photocatalytic decomposition of pollutants. In this study, the degradation efficiency of PNG was investigated in the range of 0 to 120 min of reaction time in different pollutant concentrations. According to the results, the degradation rate of PNG was the highest in the first 20 min and was almost constant after 20 min. In the first stages of decomposition, due to the high number of empty holes on the surface of NiFe₂O₄@TiO₂ nanocomposite and the high number of hydroxyl radicals in the solution, the degradation rate of PNG is high. But with the passing of time, these holes are filled by PNG. As a result, the amount of destruction is less than the initial stages (Derakhshani and Naghizadeh 2023, Chakrabarti et al. 2009; Alam et al. 2023).

Conclusion

This study was conducted to investigate the effect of NiFe₂O₄@TiO₂ magnetic nanocomposite as a photocatalyst in aqueous solutions. Examining the results of TEM, FTIR, XRD, FESEM, VSM, and DLS analyses confirmed that this nanocomposite was successfully synthesized and its size was about 70 nm. A green synthesis method using *Pulicaria Gnaphalodes* extract was used to prepare this nanocomposite. The results of PNG decomposition by NiFe₂O₄@TiO₂ nanocomposite showed that in optimal conditions (pH = 9, nanocomposite dose: 0.6 g/L, and PNG concentration: 10 mg/L), the highest removal efficiency was 71%. Therefore, NiFe₂O₄@TiO₂ nanocomposite has high photocatalytic activity and can effectively eliminate PNG from aqueous solutions using UV light.

Acknowledgements This article is part of the PhD thesis on Environmental Health Engineering that was approved by Birjand University of Medical Sciences (Tracking code: 456905). The authors want to acknowledge the never-ending support of the university.

Authors Contributions All authors contributed to the study conception and design. Material preparation, data collection and analysis were done by ED and AN. The synthesis of the nanocomposite was done by ED and SM. The first draft of the manuscript was written by ED. All authors read and approve the final manuscript.

Funding This work was supported by Birjand University of Medical Sciences.

Data availability All data generated or analyzed during this study are included in this published article.

Declarations

Conflicts of interest All authors declare they have no competing interests.

Ethical approval This article does not contain any studies with human participants or animals performed by any of the authors.

Consent to participate This section is “not applicable” for this study, as the study does not involve any human participants or their data or biological material.

Consent to publish All the authors mentioned in the manuscript have agreed to authorship, read, and approved the manuscript, and given consent for submission and subsequent publication of the manuscript.

Open Access This article is licensed under a Creative Commons Attribution 4.0 International License, which permits use, sharing, adaptation, distribution and reproduction in any medium or format, as long as you give appropriate credit to the original author(s) and the source, provide a link to the Creative Commons licence, and indicate if changes were made. The images or other third party material in this article are included in the article's Creative Commons licence, unless indicated otherwise in a credit line to the material. If material is not included in the article's Creative Commons licence and your intended use is not permitted by statutory regulation or exceeds the permitted use, you will need to obtain permission directly from the copyright holder. To view a copy of this licence, visit <http://creativecommons.org/licenses/by/4.0/>.

References

- Ahmed MB, Zhou JL, Ngo HH, Guo W (2015) Adsorptive removal of antibiotics from water and wastewater: progress and challenges. *Sci Total Environ* 532:112–126
- Aksu Z, Dede O (2005) Application of biosorption for Penicillin G removal: comparison with activated carbon. *Process Biochem* 40:831–847
- Alam U, Fleisch M, Kretschmer I, Bahnemann D, Muneer M (2017) One-step hydrothermal synthesis of Bi-TiO₂ nanotube/graphene composites: an efficient photocatalyst for spectacular degradation of organic pollutants under visible light irradiation. *Appl Catal B* 218:758–769
- Alam U, Khan A, Ali D, Bahnemann D, Muneer M (2018) Comparative photocatalytic activity of sol-gel derived rare earth metal (La, Nd, Sm And Dy)-doped ZnO photocatalysts for degradation of dyes. *RSC Adv* 8:17582–17594
- Alam U, Pandey A, Verma N (2023) An anthraquinone-Integrated S-scheme-based Nitro3-G-C₃N₄ composite with enhanced hydrogen production activity. *Int J Hydrogen Energy* 48:2532–2541
- Anirudhan TS, Manjusha V, Shainy F (2021) Magnetically retrievable cysteine modified graphene Oxide@Nickelferrite@Titanium dioxide photocatalyst for the effective degradation of chlorpyrifos from aqueous solutions. *Environ Technol Innov* 23:101633
- Arsand DR, Kümmerer K, Martins AF (2013) Removal of dexamethasone from aqueous solution and hospital wastewater by electrocoagulation. *Sci Total Environ* 443:351–357
- Basha S, Barr C, Keane D, Nolan K, Morrissey A, Oelgemöller M, Tobin JM (2011) On the adsorption/photodegradation of amoxicillin in aqueous solutions by an integrated photocatalytic adsorbent (IPCA): experimental studies and kinetics analysis. *Photochem Photobiol Sci* 10:1014–1022
- Bousquet-Berthelin C, Chaumont D, Stuerger D (2008) Flash microwave synthesis of trevorite nanoparticles. *J Solid State Chem* 181:616–622
- Chakrabarti S, Chaudhuri B, Bhattacharjee S, Ray AK, Dutta BK (2009) Photo-reduction of hexavalent chromium in aqueous solution in the presence of zinc oxide as semiconductor catalyst. *Chem Eng J* 153:86–93

- Darvishi Cheshmeh Soltani R, Rezaee A, Safari M, Khataee AR, Karimi B (2015) Photocatalytic degradation of formaldehyde in aqueous solution using ZnO nanoparticles immobilized on glass plates. *Desalin Water Treat* 53:1613–1620
- Dehghani M, Nasserri S, Ahmadi M, Samaei MR, Anushiravani A (2014) Removal of Penicillin G from aqueous phase by Fe+3-TiO₂/UV-A process. *J Environ Health Sci Eng* 12:56
- Derakhshani E, Naghizadeh A (2023) Recent advancement in NiFe₂O₄-based nanocomposites for the photocatalytic degradation of pollutants in aqueous solutions: a comprehensive systematic review. *Aqua Water Infrastruct Ecosyst Soc* 72(8):1629–1645
- Derakhshani E, Naghizadeh A, Arab-Zozani M, Farkhondeh T (2023a) A systematic review of photocatalytic degradation of humic acid in aqueous solution using nanoparticles. *Rev Environ Health* 38:577–587
- Derakhshani E, Naghizadeh A, Mortazavi-Derazkola S (2023b) Biosynthesis of MnFe₂O₄@ TiO₂ magnetic nanocomposite using Oleaster tree bark for efficient photocatalytic degradation of Humic acid in aqueous solutions. *Environ Sci Pollut Res* 30:3862–3871
- Elmolla ES, Chaudhuri M (2010) Photocatalytic degradation of amoxicillin, ampicillin and cloxacillin antibiotics in aqueous solution using UV/TiO₂ and UV/H₂O₂/TiO₂ photocatalysis. *Desalination* 252:46–52
- Esmati M, Allahresani A, Naghizadeh A (2021) Synthesis and characterization of graphitic carbon nitride/mesoporous nano-silica (G-C₃N₄/Kcc-1) nanocomposite as a novel highly efficient and recyclable photocatalyst for degradation of antibiotic in aqueous solution. *Res Chem Intermed* 47:1447–1469
- Geng N, Chen W, Xu H, Ding M, Liu Z, Shen Z (2019) A Sono-photocatalyst for humic acid removal from water: operational parameters, kinetics and mechanism. *Ultrason Sonochem* 57:242–252
- Gulkowska A, Leung HW, So MK, Taniyasu S, Yamashita N, Yeung LW, Richardson BJ, Lei AP, Giesy JP, Lam PK (2008) Removal of antibiotics from wastewater by sewage treatment facilities In Hong Kong and Shenzhen, China. *Water Res* 42:395–403
- Hirai T, Kobayashi J, Komazawa I (1999) Preparation of acicular ferrite fine particles using an emulsion liquid membrane system. *Langmuir* 15:6291–6298
- Hussain I, Singh NB, Singh A, Singh H, Singh SC (2016) Green synthesis of nanoparticles and its potential application. *Biotech Lett* 38:545–560
- Kamranifar M, Allahresani A, Naghizadeh A (2019a) Application of CoFe₂O₄@Cus magnetic nanocomposite as a novel adsorbent for removal of Penicillin G from aqueous solutions: isotherm, kinetic and thermodynamic study. *Desalin Water Treat* 148:263–273
- Kamranifar M, Allahresani A, Naghizadeh A (2019b) Synthesis and characterizations of a novel CoFe₂O₄@ Cus magnetic nanocomposite and investigation of its efficiency for photocatalytic degradation of Penicillin G antibiotic in simulated wastewater. *J Hazard Mater* 366:545–555
- Karmakar S, Routray KL, Panda B, Sahoo B, Behera D (2018) Construction of Core@Shell nanostructured NiFe₂O₄@TiO₂ ferrite nand logic gate using fluorescence quenching mechanism for TiO₂ sensing. *J Alloys Compound* 765:527–537
- Kim HS, Kim D, Kwak BS, Han GB, Um M-H, Kang M (2014) Synthesis of magnetically separable Core@Shell structured NiFe₂O₄@ TiO₂ nanomaterial and its use for photocatalytic hydrogen production by methanol/water splitting. *Chem Eng J* 243:272–279
- Kulkarni G, Patade S, Parlikar R, Chilwar R, Saraf T, Jadhav K (2020) Green synthesis of NiFe₂O₄ nanoparticles using different fuels and their structural characterization. *J Phys Conf Series* 2020:012003
- Li H, Wu H-Z, Xiao G-X (2010) Effects of synthetic conditions on particle size and magnetic properties of NiFe₂O₄. *Powder Technol* 198:157–166
- Li R, Jia Y, Wu J, Zhen Q (2015) Photocatalytic degradation and pathway of oxytetracycline in aqueous solution by Fe₂O₃-TiO₂ nanopowder. *RSC Adv* 5:40764–40771
- Lima LM, Silva BNMD, Barbosa G, Barreiro EJ (2020) B-lactam antibiotics: an overview from a medicinal chemistry perspective. *Eur J Med Chem* 208:112829
- Makofane A, Maake PJ, Mathipa MM, Matinise N, Cummings FR, Motaung DE, Hintsho-Mbita NC (2022) Green synthesis of NiFe₂O₄ nanoparticles for the degradation of methylene blue, sulfisoxazole and bacterial strains. *Inorg Chem Commun* 139:109348
- Malik R, Annapoorani S, Lamba S, Reddy VR, Gupta A, Sharma P, Inoue A (2010) Mössbauer and magnetic studies in nickel ferrite nanoparticles: effect of size distribution. *J Magnet Magnet Mater* 322:3742–3747
- Moradi S, Taghavi Fardood S, Ramazani A (2018) Green synthesis and characterization of magnetic NiFe₂O₄@ ZnO nanocomposite and its application for photocatalytic degradation of organic dyes. *J Mater Sci Mater Electron* 29:14151–14160
- Naghizadeh A, Nasserri S, Mahvi AH, Nabizadeh R, Kalantary RR (2015) Fenton regeneration of humic acid-spent carbon nanotubes. *Desalin Water Treat* 54:2490–2495
- Naghizadeh A, Momeni F, Derakhshani E (2017) Efficiency of ultrasonic process in regeneration of graphene nanoparticles saturated with humic acid. *Desalin Water Treat* 70:290–293
- Ouaissa YA, Chabani M, Amrane A, Bensmaili A (2014) Removal of tetracycline by electrocoagulation: kinetic and isotherm modeling through adsorption. *J Environ Chem Eng* 2:177–184
- Pandey A, Alam U, Gupta A, Shim J-J (2023) S-Scheme Heterojunction-mediated hydrogen production over the graphitic carbon nitride-anchored nickel stannate perovskite. *Fuel* 355:129538
- Poursaberi T, Hassanisad M, Torkestani K (2012) The synthesis of magnetite nanoparticles functionalized by Nb (V) metalloporphyrin for the selective removal of fluoride ions from aqueous media. *J Water Soil Resour Cons* 1:71–83
- Qin K, Zhao Q, Yu H, Xia X, Li J, He S, Wei L, An T (2021) A Review of bismuth-based photocatalysts for antibiotic degradation: insight into the photocatalytic degradation performance pathways and relevant mechanisms. *Environ Res* 199:111360
- Saif S, Tahir A, Chen Y (2016) Green synthesis of iron nanoparticles and their environmental applications and implications. *Nanomaterials* 6:209
- Salehnia S, Barikbin B, Khosravi R (2020) Removal of Penicillin G by electro-fenton process from aqueous solutions. *J Res Environ Health* 6:23–33
- Sanadi K, Rathod K, Gaur M, Powar R, Parale V, Patil R, Burungale S, Mali A (2021) UV light-activated photocatalytic degradation of rhodamine B dye and suzuki cross-coupling reaction by Ni ferrite catalyst synthesized by sol-gel auto-combustion method. *Bull Mater Sci* 44:1–8
- Seifrtová M, Nováková L, Lino C, Pena A, Solich P (2009) An overview of analytical methodologies for the determination of antibiotics in environmental waters. *Anal Chim Acta* 649:158–179
- Singh A, Alam U, Chakraborty P, Sundararaju B, Verma N (2023) A sustainable approach for the production of formate from CO₂ using microalgae as a clean biomass and improvement using potassium-doped G-C₃N₄. *Chem Eng J* 454:140303
- Sivakumar P, Ramesh R, Ramanand A, Ponnusamy S, Muthamizhchelvan C (2011) Preparation of sheet like polycrystalline NiFe₂O₄ nanostructure with PVa matrices and their properties. *Mater Lett* 65:1438–1440
- Sivakumar P, Ramesh R, Ramanand A, Ponnusamy S, Muthamizhchelvan C (2013) Synthesis and characterization of NiFe₂O₄ nanoparticles and nanorods. *J Alloys Compound* 563:6–11

- Sui Q, Huang J, Deng S, Yu G, Fan Q (2010) Occurrence and removal of pharmaceuticals, caffeine and deet in wastewater treatment plants of Beijing, China. *Water Res* 44:417–426
- Sun J, Song M, Feng J, Pi Y (2012) Highly efficient degradation of Ofloxacin by UV/Oxone/CO₂+ oxidation process. *Environ Sci Pollut Res Int* 19:1536–1543
- Wammer KH, Korte AR, Lundeen RA, Sundberg JE, Mcneill K, Arnold WA (2013) Direct photochemistry of three fluoroquinolone antibacterials: Norfloxacin, Ofloxacin, and Enrofloxacin. *Water Res* 47:439–448
- Wang J, Zhuan R (2020) Degradation of antibiotics by advanced oxidation processes: an overview. *Sci Total Environ* 701:135023
- Wang Y-W, Yuan P-H, Fan C-M, Wang Y, Ding G-Y, Wang Y-F (2012) Preparation of Zinc titanate nanoparticles and their photocatalytic behaviors in the photodegradation of humic acid in water. *Ceram Int* 38:4173–4180
- Yan W, Jiang W, Zhang Q, Li Y, Wang H (2010) Structure and magnetic properties of nickel-zinc ferrite microspheres synthesized by solvothermal method. *Mater Sci Eng B* 171:144–148
- Zhao H, Zheng Z, Wong KW, Wang S, Huang B, Li D (2007) Fabrication and electrochemical performance of nickel ferrite nanoparticles as anode material in lithium ion batteries. *Electrochem Commun* 9:2606–2610

Publisher's Note Springer Nature remains neutral with regard to jurisdictional claims in published maps and institutional affiliations.